Modelling and simulation of saturation region in double gate Graphene nanoribbon transistors

© Mahdiar Ghadiry¶, Mahdieh Nadi*, Meysan Rahmani+, Mohamad Ahmadi+, Asrulnizam Abd Mahaf

School of Electrical and Electronic Engineering, Engineering Campus, University Sains Malaysia, Penang, Malaysia
* Department of Computer Engineering, Ashtian Branch, Islamic Azad University, Ashtian, Iran
+ Faculty of Electrical and Electronics, University Technologi Malaysia, Skudai, Malaysia

(Получена 23 мая 2011 г. Принята к печати 28 июня 2011 г.)

A novel analytical model for surface field distribution and saturation region length for double gate graphene nanoribbon transistors has been proposed. The solution for surface potential and electric field has been derived based on Poisson equation. Using the proposed models, the effects of several parameters such as drain–source voltage, oxide thickness and channel length on the length of saturation region and electric field near the drain have been studied.

1. Introduction

Demand for high-speed performance in memory and logic applications caused continuous shrinking in devices' dimensions. To continue this scaling trend the channel length of silicon MOSFETs as predicted by ITRS will need to be scaled even further to meet future generation technology requirements [1]. However, there are some uncertainties about the behaviour of the existing Si devices under extreme scaling. Therefore, several device concepts have been proposed, such as nanowire FETs, carbon nanotube field effect transistors (CNT FETs), graphene nanoribbon FET, etc. Among these devices, CNT FETs have been extensively studied and generated considerable interest due to their unique electronic properties, especially their very high carrier mobility and conductance [1]. However, there are still some unresolved issues about uniformly control on the chirality of CNTs, making them questionable to use in realistic applications [1]. Recent experemental studies [2], show the possibility of fabricating graphene nanoribbon (GNR) transistors, and the potential of GNRs as an alternative material to bypass the CNT chirality challenges while still preserve the excellent electronic properties such as light effective mass and high electron/hole mobility [1]. As a result, many researchers have been attracted to this area and provided several models for GNR transistors' properties [3,4] and applications [5,6]. Nevertheless, there is lack of research in modelling their behaviour near the drain junction and their breakdown voltage.

The velocity-saturation-region length (LVSR) of FETs is one of the most important parameters in short-channel devices. It governs the drain breakdown voltage [7,8], substrate current, hot-electron generation [9,10] and drain current at velocity saturation region [11–13]. In a FET, if the drain voltage exceeds the saturation drain voltage, the electric field near the drain region will exceed the critical field strength for causing carrier velocity saturation [14]. The high field strength in this region also causes impact ionization and substrate current generation [14].

In a short-channel device, the high field region becomes the major portion of channel and governs the current flow. In order to gain insights into reliability issues of these devices, close analysis of this region is necessary. In addition, these kinds of models open the way to design power transistors based on graphene.

Since there is no experimental data to show the effect of different parameters on the length of this region, analytical modelling seems to be a powerful tool in this case. Therefore, firstly, we provide simple models for surface potential and electric field distribution of double gate GNR FET. Secondly, we extract the LVSR model from the proposed surface potential model.

This paper is organized as follows: section 2 derives and explains the proposed model; section 3 shows the results and discuses them and finally section 4 concludes this paper.

2. The proposed model for LVSR

A schematic cross-section of double gate GNR FET is shown in Fig. 1, where t_{ox} is the oxide thickness of top gate

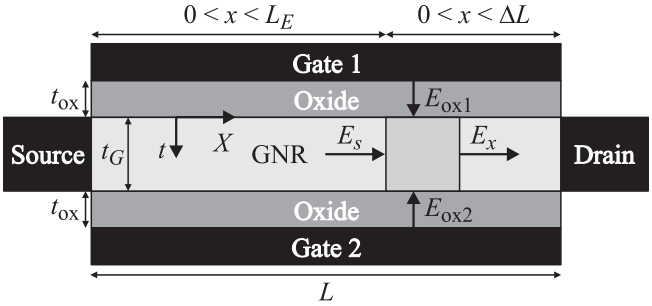

Рис. 1. Schematic cross section of a double gate GNR FET [15]. Typical device parameters are: doping concentration $N_d = 5 \cdot 10^{16}\,\mathrm{m}^{-2}$, $t_{ox} = 1\,\mathrm{nm}$, $L = 20\,\mathrm{nm}$, and $w_G = 5\,\mathrm{nm}$ [4].

¶ E-mail: m.hoseinghadiry@gmail.com

with dielectric constant of ε_{ox}; t_G, w_G and L are the GNR's thickness, width and the channel length respectively.

Applying Gauss law for the device presented in Fig. 1 yields

$$-\int_0^x \varepsilon_{ox}E_{ox1}dx - \int_0^x \varepsilon_{ox}E_{ox2}dx - \int_0^{t_G} \varepsilon_G E_s dt + \int_0^{t_G} \varepsilon_G E(x)dt = -q\int_0^x\int_0^{t_G}(n+N_d)dxdt, \quad (1)$$

where E_s is the surface electric at onset of saturation region, ε_G and ε_{ox} are GNR and oxide dielectric constants, E_{ox} is the electric field of the oxide.

By solving Eq. (1) and taking $E_{ox}(x) = [V_G - V_{BI} - V(x)]/t_{ox}$, Eq. (2) is obtained:

$$\frac{d^2V(x)}{dx} - \frac{V(x)}{2\lambda^2} + \frac{(V_G - V_{BI})}{2\lambda^2} = \frac{q(n+N_d)}{\varepsilon_G}, \quad (2)$$

where, $V(x)$ is the surface potential of GNR at any point along the x direction inside the saturation region $(0 < x < \Delta L)$, $V_G = 0.5\,\mathrm{V}$ is top gate and back gate voltage, and q is charge magnitude. The parameter $\lambda = (\varepsilon_G t_G t_{ox}/\varepsilon_{ox})^{-2}$ is relevant length scale for potential variation [16]. Built-in voltage V_{BI} in GNR with a bandgap $E_G = hV_F/3w_G$ [17] can be calculated using Eq. (3),

$$V_{BI} = \frac{hv_F}{6qw_G} - V_T \ln\left(\frac{N}{n_i}\right), \quad (3)$$

where, $v_F \approx 10^6$ m/s is the Fermi velocity, $V_T = k_B T/q$ is thermal voltage, n_i and N are the intrinsic and doping carrier concentration.

Boundary conditions for Eq. (2) can be defined as $V(0) = V_s$, $V(\Delta L) = V_D$, $E(0) = E_s$, where V_s, V_D, ΔL are saturation voltage at onset of saturation region, drain voltage and length of saturation velocity region (LVSR) respectively [18]. Solving Eq. (2) with the defined boundary conditions and taking

$$A = -\frac{q(N_d+n)}{\varepsilon_G} - \frac{V_G - V_{BI}}{2\lambda^2}$$

yields

$$V(x) = -2\lambda^2 A + (2\lambda^2 A + V_s)\,\mathrm{ch}\left(\frac{x}{\sqrt{2}\lambda}\right) + \sqrt{2}\lambda E_s\,\mathrm{sh}\left(\frac{x}{\sqrt{2}\lambda}\right). \quad (4)$$

Since $E(x) = -dV(x)/dx$, the surface electric field distribution $E(x)$ can simply be obtained using Eq. (4).

$$|E(x)| = \left(\sqrt{2}\lambda A + \frac{V_s}{\sqrt{2}\lambda}\right)\mathrm{sh}\left(\frac{x}{\sqrt{2}\lambda}\right) + E_s\,\mathrm{ch}\left(\frac{x}{\sqrt{2}\lambda}\right). \quad (5)$$

For the cases where $x/\lambda > 4$ (near the drain region) $\mathrm{sh}(x/\lambda)$ and $\mathrm{ch}(x/\lambda)$ can be approximated to $0.5\exp(x/\lambda)$. Therefore, Eqs (4) and (5) are reduced to

$$V(x) \approx 0.5\left(2\lambda^2 A + V_s + \sqrt{2}\lambda E_s\right)\exp\left(\frac{x}{\sqrt{2}\lambda}\right) - 2\lambda^2 A, \quad (6)$$

$$|E(x)| \approx 0.5\left(\sqrt{2}\lambda A + \frac{V_s}{\sqrt{2}\lambda} + E_s\right)\exp\left(\frac{x}{\sqrt{2}\lambda}\right). \quad (7)$$

In order to calculate ΔL, either Eq. (4) or (6) can numerically be solved at $x = \Delta L$. For example, using Eq. (6) we have

$$\Delta L \approx L - \frac{\lambda V_s \frac{1}{\sqrt{2}}\exp\left(\frac{\Delta L}{\sqrt{2}\lambda}\right)}{V_D + 2\lambda^2 A - \frac{1}{2}\exp\left(\frac{\Delta L}{\sqrt{2}\lambda}\right)(2\lambda^2 A + V_s)}. \quad (8)$$

Since the focus of this paper is modelling of the saturation region, the electric field between source and the saturation region $(0 < x < \Delta L)$ can be assumed to be linear for simplicity [15,18–21]. As a result it can be simply concluded that

$$d^2V(L_E)/dx^2 = -\frac{E_s}{L_E}, \quad (9)$$

where L_E is the effective channel length defined as $L_E = L - \Delta L$. Using Gauss law again inside the linear region results in a same differential Eq. as (2). Solving Eq. (2) with the new boundary condition of (9) results

$$E_s = \frac{L_E}{2\lambda^2 - L_E^2}\left(\frac{t_G t_{ox} q(N_d+n)}{\varepsilon_{ox}} + V_G - V_{BI}\right). \quad (10)$$

Since λ is much less than L_E $(0.5 < \lambda < 5\,\mathrm{nm}$ and $8 < L_E < 17\,\mathrm{nm})$ for the most cases of this study, term λ^2 in Eq. (10) can be neglected respect to L_E^2. Thus Eq. (10), can be reduced to

$$|E_s| \approx \frac{1}{L_E}\left(\frac{t_G t_{ox} qN}{\varepsilon_{ox}} + V_G + V_{BI}\right). \quad (11)$$

In addition, V_s can be computed as Eq. (12) by integrating Eq. (11) assuming the source voltage $V(0)$ equal to 0:

$$V_s \approx \frac{t_G t_{ox} qN}{\varepsilon_{ox}} + V_G + V_{BI}. \quad (12)$$

3. Results and discussion

Fig. 2 shows the electric field distribution in the lateral direction with the different drain voltages. The values for V_D have been chosen based on saturation voltage V_s, which has been almost 0.36 V in this simulation. This Figure indicates that the potential distribution along the nanoribbon surface is similar to the profile of an abrupt junction at the edges of p-base/drift region and drain/drift region junctions [22]. In other word, it shows the electric field profile follows an exponential form depending on the distance from the drain. Eq. (7) also highlighted this fact.

Fig. 3 shows the saturation electric field at different drain–source voltages, channel thicknesses and channel lengths. As can be seen increasing V_D results in slight increase in E_s. In addition, this Figure shows by increasing t_{ox} and L, saturation electric field increases and decreases respectively.

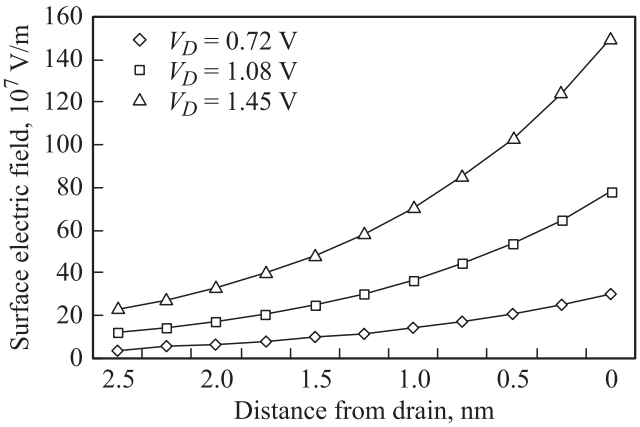

Рис. 2. Surface electric field distribution at different drain voltages.

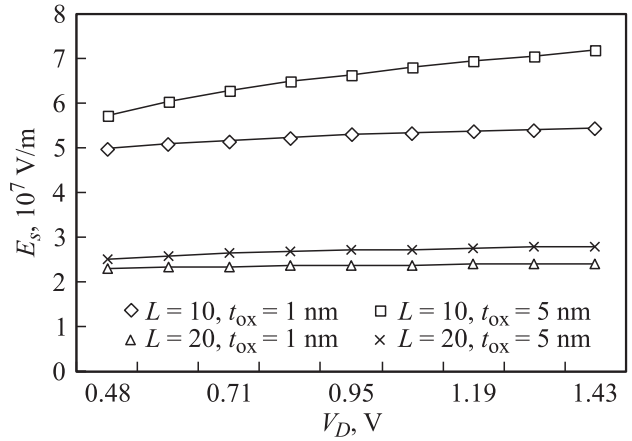

Рис. 3. Saturation electric field at different drain voltages.

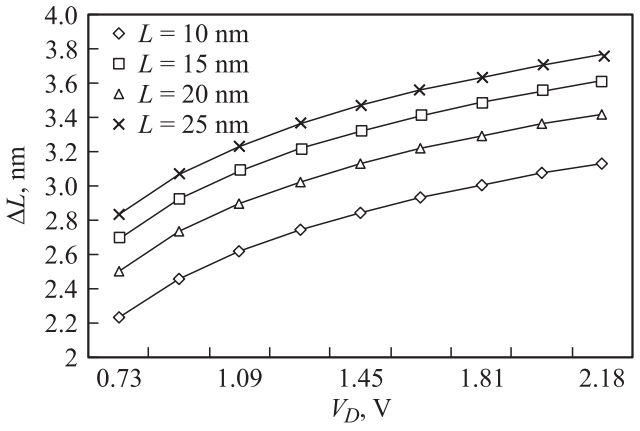

Рис. 4. The length of velocity saturation region with different channel lengths and drain voltages.

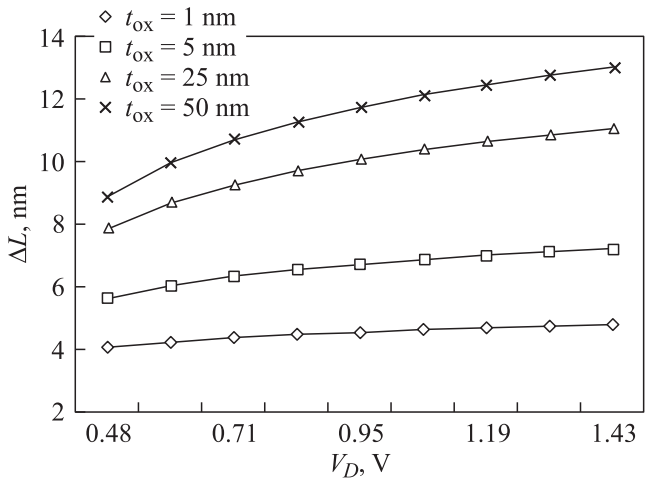

Рис. 5. The length of velocity saturation region vs. oxide thichness variations at different drain voltages.

Fig. 4 depicts the effect of the drain voltage and channel length on the length of saturation region. The higher drain voltage and longer channel the longer ΔL. In addition, the Figure shows that the ratio of $\Delta L/L$ increases as L decreases.

In Fig. 5 it can be seen that increasing the oxide thickness causes increase in ΔL. In addition, the term $d(\Delta L)/d(V_D)$ increases as t_{ox} increases.

4. Conclusion

Analytical models for surface potential, electric field and LVSR of double gate GNR transistors were proposed and the behaviour of a typical device in the saturation region was investigated using the proposed models. In addition, the effects of device parameters such as oxide thickness, and channel length were examined. The results of this model could be applicable for providing accurate design schemes and clear physical insights. In future, impact ionization coefficient and breakdown voltage of these transistors could be modelled and possibility of making power devices studied.

Acknowledgments: This work has been supported by PhD fellowship scheme with no. 1/11 and grant numbered 04/PELECT/60310023 from school of electrical and electronic engineering, University Sains Malaysia. In addition, the authors would like to thank Dr. Mehdi Khiabani for his helpful comments on deriving equations.

Список литературы

[1] G. Liang, N. Neophytou et al. J. of Comput. Electron., **7**, 394 (2008).
[2] M.C. Lemme, T.J. Echtermeyer et al. IEEE Trans. Electron. Dev. Lett., **28**, 282 (2007).
[3] M. Ahmadi, Z. Johari et al. J. Nanomaterials **2010**, 1 (2010).

[4] M. Cheli, P. Michetti, G. Iannaccone. IEEE Trans. Electron. Dev., **57**, 1939 (2010).
[5] K. Navi, M. Raswhtian et al. Nanoscale Res. Lett. **5**, 859 (2010).
[6] R. Sordan, F. Traversi, V. Russo. Appl. Phys. Lett. **94**, 1 (2009).
[7] A. Schutz, S. Selberherr, H.W. Pö tzl. Solid-State Electron., **25**, 177 (1982).
[8] H. Wong. IEEE Trans. Electron. Dev., **42**, 2197 (1995).
[9] N.D. Arora, M.S. Sharma. IEEE Trans. Electron. Dev., **38**, 1392 (1991).
[10] F.F. Fang, A.B. Fowler. J. Appl. Phys., **41**, 1825 (1970).
[11] D. Frohman-Bentchkowsky, A.S. Grove. IEEE Trans. Electron Dev., **16**, 108 (1969).
[12] G. Baum, H. Beneking. IEEE Trans. Electron. Dev., **17**, 481 (1970).
[13] G. Gildenblat, L. Xin et al. IEEE Trans. Electron. Dev., **53**, 1979 (2006).
[14] H. Wong, M.C. Poon. IEEE Trans. Electron. Dev., **44**, 2033 (1997).
[15] I. Meric, M.Y. Han et al. Nature Nanotechnology, **3** 654 (2008).
[16] H. Wong. Microelectron.i Reliab. **40**, 3 (2000).
[17] Q. Zhang, T. Fang et al. IEEE Electron. Dev. lett. **29**, 1344 (2008).
[18] M. El Banna, M. El Nokali. Solid-State Electron. **31**, 269 (1988).
[19] D. Krizaj, G. Charitat, S. Amon. Solid-State Electron. **39**, 1353 (1996).
[20] J.S. Kolhatkar, A.K. Dutta. IEEE Trans. Electron. Dev., **47**, 861 (2000).
[21] A.K. Singh. Microelectron. International, **22**, 16 (2005).
[22] W. Yang, X. Cheng et al. Solid-State Electron. **49**, 43 (2005).

Редактор Т.А. Полянская